International Journal of Applied Power Engineering (IJAPE)
Vol. 15, No. 1, March 2026, pp. 383~392
ISSN: 2252-8792, DOI: 10.11591/ijape.v15.i1.pp383-392

Sensorless control strategy for brushless doubly fed reluctance generator under voltage flickering at point of common coupling

Manish Paul[1,2], Adikanda Parida[1], Anu Kumar Das[1]
[1]Department of Electrical Engineering, North Eastern Regional Institute of Science and Technology, Nirjuli, India
[2]Department of Electrical Engineering, ICFAI University, Tripura, India

Article Info

Article history:

Received Apr 20, 2025
Revised Dec 2, 2025
Accepted Jan 9, 2026

Keywords:

Microgrids
Model reference adaptive system
Point of common coupling
Reluctance generator
Rotor position computation

ABSTRACT

The brushless doubly-fed reluctance generator (BDFRG) is widely used in grid-connected wind energy conversion systems (WECS). It has been observed that there is a continuous voltage flickering at the point of common coupling (PCC) between the BDFRG power terminals and the alternating current (AC) microgrids due to either the load variations or wind turbine output variations. Under such circumstances, sensorless control of BDFRG using the existing model reference adaptive system (MRAS) models exhibits erroneous active power output. This is because the variables selected in these models are directly or indirectly dependent on the voltage at the PCC. In this paper, a sensorless control mechanism for the BDFRG is proposed, which provides better performance in terms of control accuracy. Moreover, the planned scheme is insensitive to the parameter variations of the BDFRG. The performance of the planned system has been tested with a voltage flickering of 50% for 1 ms at the PCC. The stability test presented in this paper reveals that the model is robust and error-free against the noise disturbances. The planned system is implemented using proper simulations and a hardware platform with a practical BDFRG of 2.5 kW, and a dSPACE CP1104 module.

Corresponding Author:

Adikanda Parida
Department of Electrical Engineering, North Eastern Regional Institute of Science and Technology
Nirjuli, Arunachal Pradesh, India
Email: adikanda_2003@yahoo.co.in

NOMENCLATURE

ω_r	:	Speed of the rotor	R_p, R_s	:	Primary, secondary winding resistances
ω_p	:	Speed of primary winding flux	L_p	:	Primary winding self-inductance
ω_s	:	Speed of secondary winding flux	L_s	:	Secondary winding self-inductance
V_{pd}, V_{pq}	:	Two-axis primary winding voltages	i_{sd}, i_{sq}	:	Dq-axis secondary winding currents
V_{sd}, V_{sq}	:	Two-axis secondary winding voltages	P_p, P_s	:	Primary, secondary winding active power
i_{pd}, i_{pq}	:	Two-axis primary winding currents	λ_p, λ_s	:	Primary, secondary flux
L_m	:	Mutual inductance between the primary and secondary winding	Superscript	:	*E, s, p*; synchronous, secondary, and primary reference frames

1. INTRODUCTION

The wind energy conversion system using a doubly-fed induction generator (DFIG) is a time-tested practice. However, the limitations like higher maintenance costs and power loss due to slip-rings are the major issues. Moreover, the brushless doubly-fed reluctance generator (BDFRG) is simple in construction, robust in terms of control, and exhibits improved efficiency [1]-[3] in comparison to DFIG. In terms of power delivery, the primary winding of the BDFRG is directly coupled with the grid at the point of common coupling (PCC), and the control winding is coupled with the utility through a back-to-back converter [4], [5]. For the active and reactive powers of the BDFRG, two flux-oriented vector control technique for BDFRG is suggested in [6], [7]. Appropriate scalar control techniques are suggested in [8] and [9]. Also, various vector control mechanisms are presentedin [10]-[15]. However, the techniques presented in [6]-[15], including the other non-referenced papers, do not consider sensorless controls even though a large number of sensorless control methods of DFIG are available as presented in [16]-[24].

The sensorless model reference adaptive system (MRAS) technique presented in [25] for BDFRG control uses stator flux as the variable, and the terminal voltage is associated with the reference variable only. Similarly, the model reference adaptive system (MRAS) technique used for the same purpose in [26] uses active power as the variable, and the terminal voltage is associated with an adjustable variable only. Therefore, the voltage flickering at the point of common coupling (PCC) will severely introduce errors in the rotor speed estimation process. The sensorless control mechanism presented in this paper uses a MRAS technique for the estimation of BDFRG rotor speed and position, considering the real power of the machine as the adaptable variable. However, the terminal voltage is associated with both the reference and the adjustable variable. Therefore, the effect due to voltage flickering at PCC will be nullified, and the estimation process is found to be error-free. Moreover, the planned model is not sensitive to the machine parameter variations. The highlighted contributions of the planned sensorless control technique are summarized as follows:

i) The uniqueness of the proposed sensorless control technique for the BDFRG is that it effectively performs under voltage flickering at the PCC between power terminals and the microgrids.
ii) The proposed sensorless technique is insensitive to the parameter variations of the BDFRG.
iii) The proposed MRAS model is stable against any noise disturbances.

2. METHODOLOGY AND THE PROPOSED CONTROLLER

The planned controller in this paper has been presented through sensorless rotor position estimation of the BDFRG. The accuracy of the controller for machine parameter variations and flickering at PCC has also been tested. The robustness of the planned controller towards noise disturbances has been tested and appropriately presented. The overall structure of the BDFRG-based wind energy generation system is as shown in Figure 1, where the primary winding of BDFRG handles power at utility frequency, and the control winding operates at the rotor frequency. The two-axis primary winding voltage equation is presented in (1) and that of the control winding in (2) in the e-reference frame, and Figure 2 as follows:

$$V_{pd}^{e} = -\omega_p \lambda_{pq}^{e}; V_{pq}^{e} = \omega_p \lambda_{pd}^{e} \tag{1}$$

$$V_{sd}^{e} = R_s i_{sd}^{e} + \frac{d\lambda_{sd}^{e}}{dt} - (\omega_p - \omega_s)\lambda_{sq}^{e};\ V_{sq}^{e} = R_s i_{sq}^{e} + \frac{d\lambda_{sq}^{e}}{dt} + (\omega_p - \omega_s)\lambda_{sd}^{e} \tag{2}$$

the two-axis primary winding currents are expressed as (3).

$$i_{pd}^{e} = \frac{(\lambda_{pd}^{e} - L_m i_{sd}^{e})}{L_p};\ \ i_{pq}^{e} = \frac{(\lambda_{pq}^{e} + L_m i_{sq}^{e})}{L_p} \tag{3}$$

The control winding current can be expressed as (4).

$$i_{sd}^{e} = \frac{(\lambda_{sd}^{e} - L_m i_{pd}^{e})}{L_s};\ \ i_{sq}^{e} = \frac{(\lambda_{sq}^{e} + L_m i_{pq}^{e})}{L_s} \tag{4}$$

The energy conversion between the control winding and the utility needs the information regarding rotor speed and position to control the stator side converter (SSC) and grid side converter (GSC). The quantity and the direction of active power flow accuracy depend on the accurate computation of the brushless doubly-fed reluctance generator (BDFRG) rotor speed and the position. Moreover, measurement of the above quantities using sensors is always erroneous and not cost effective. Therefore, in this paper, an attempt has been made to compute these quantities through an effective sensorless mechanism that is sustainable to machine parameter variations and voltage flicker at the PCC.

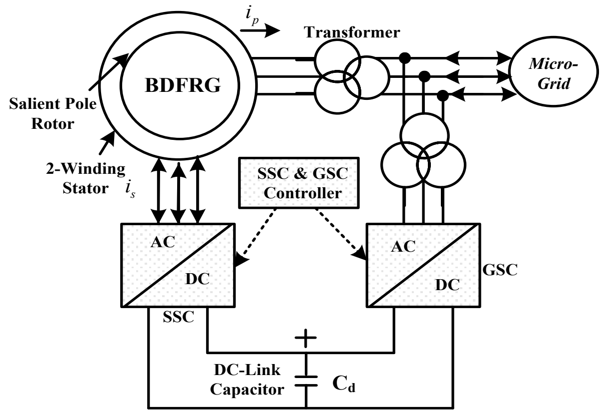

Figure 1. Basic structure

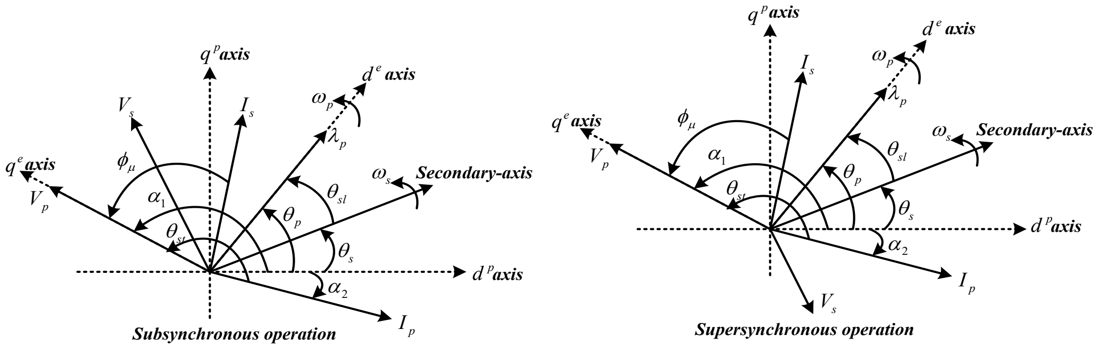

Figure 2. Primary and control winding phasor of the BDFRG

2.1. Algorithms for sensorless computation of rotor position

When the wind generator is synchronized with the microgrid, voltage flickers at the PCC are inherently reflected in the output of the voltage sensors used in almost all types of available sensorless schemes. In this paper, a modest MRAS-based model has been proposed for the computation of the rotor position of the BDFRG, which is unbiased to the voltage flickers at the PCC. To develop the planned MRAS model, the real power of the BDFRG is considered as the adaptable variable. The BDFRG active power can be expressed as (5).

$$P_p = \frac{3}{2}\left[V_{pd}^e i_{pd}^e + V_{pq}^e i_{pq}^e\right] \quad (5)$$

Substituting from (3) in (5), the BDFRG real power, and substituting $V_{pd}^e = -\omega_p \lambda_{pq}^e; V_{pq}^e = \omega_p \lambda_{pd}^e$ at steady state can be expressed as (6).

$$P_p = \frac{3}{2}(1 - \chi_s)\left[V_{pq}^e i_{sq}^e - V_{pd}^e i_{sd}^e\right] \quad (6)$$

Where χ_s is the primary winding leakage factor, and its value is almost 0.

Therefore, signifying the reference and adjustable variable for the proposed MRAS model as P_p^{ref} $\hat{P}_p$, from (5) and (6).

$$P_p^{ref} = \frac{3}{2}\left[V_{pd}^e i_{pd}^e + V_{pq}^e i_{pq}^e\right]$$
$$\hat{P}_p = \frac{3}{2}\left[V_{pq}^e i_{sq}^e - V_{pd}^e i_{sd}^e\right] \quad (7)$$

Since the primary winding is directly coupled with PCC, for any voltage variation at PCC, the stator voltage of the BDFRG will vary. However, it can be observed from (7) that in the planned MRAS model, both the reference as well as the adaptable variables are associated with the primary winding voltage. Therefore, the voltage flicker at the PCC is ineffective in the case of the planned scheme. Hence, the computation of the BDFRG rotor position and the speed is error-free. The planned model can be observed from Figure 3, and the output can be observed from Figure 4.

The performance of the presented scheme under variable wind speed conditions can be observed from Figure 4(a), where BDFRG rotor speed was computed using the presented MRAS model and compared with the measured value with almost zero computational error. Similarly, from Figure 4(b), it can be observed that the planned MRAS model effectively computes the rotor position, and the same has been compared with its measured value. It has been observed that the planned model accurately computes the BDFRG rotor position. From (7), it can be observed that the adjustable variable $\hat{P}_p$ is free from any machine parameter dependencies. It has been observed that if the adjustable variable is coupled with L_m of the BDFRG, the performance of the MRAS model will be erroneous. Because L_m is a continuously varying parameter in case of BDFRG. If the L_m value is fixed without updating the mechanism, the computation of the BDFRG rotor position will be erroneous. However, the planned scheme is free from any parameter dependencies and hence more accurate. The effectiveness of the planned scheme has been tested for the L_m variation between -50% to +50% as shown in Figures 5(a) and 5(b), respectively. It can be seen in Figures 5(a) and 5(b) that the planned model computes the rotor speed and position very accurately with very insignificant errors. Similarly, the primary winding resistance R_p has been varied by 50% as shown in Figures 5(c) and 5(d). It can be observed from Figure 5(c) that BDFRG rotor position computation using the is very accurate when R_p the value is increased by 50%. In Figure 5(d), the performance of the planned MRAS model is satisfactory, where the R_p value decreased by 50%.

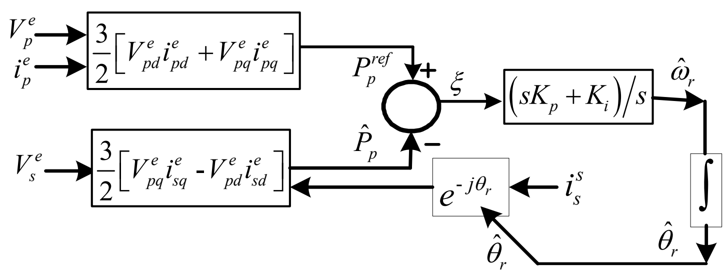

Figure 3. Proposed MRAS model

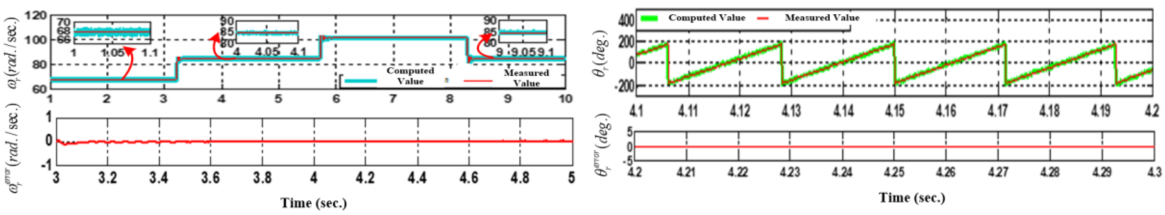

Figure 4. Performance of the proposed MRAS model: (a) computation of BDFRG rotor speed and (b) computation of BDFRG rotor position

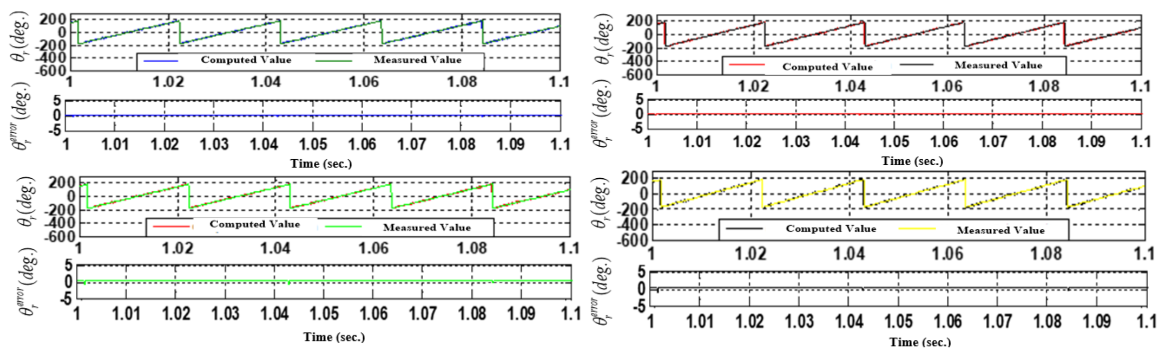

Figure 5. BDFRG rotor position computation by the proposed MRAS model with (a) L_m variation by -50%, (b) L_m variation by +50%, (c) R_p variation by +50%, and (d) R_p variation by -50%

2.2. Stability test of the proposed MRAS model

The stability of the proposed algorithm has been tested through a small signal model as shown in Figure 6 [27]. From (7), the error ξ can be expressed in a synchronous reference frame as (8).

$$\xi = P_p^{ref} - \hat{P}_p = \frac{3}{2}\left[\left(V_{pd}^e i_{pd}^e + V_{pq}^e i_{pq}^e\right) - \left(V_{pq}^e i_{sq}^e - V_{pd}^e i_{sd}^e\right)\right] \tag{8}$$

Aligning primary stator voltage along d^e-axis, V_{pq}^e= 0, the torque error signal can be expressed as (9).

$$\xi = \frac{3}{2}\left[\left(V_{pd}^e i_{pd}^e\right) + \left(V_{pd}^e i_{sd}^e\right)\right] \tag{9}$$

Therefore, change in error $\Delta\xi$ can be expressed as (10).

$$\Delta\xi = \frac{3}{2}\left[\left(V_{pd0}^e \Delta i_{pd}^e + \Delta V_{pd}^e i_{pd0}^e\right) + \left(V_{pd0}^e \Delta i_{sd}^e + \Delta V_{pd}^e i_{sd0}^e\right)\right] \tag{10}$$

From (1), for constant flux operation, $\Delta V_{pd}^e = 0$ and $\Delta i_{pd}^e = 0$ for constant torque operation. Thus, from (10):

$$\Delta\xi = \frac{3}{2} V_{pd0}^e \Delta i_{sd}^e \tag{11}$$

if $\widehat{\omega} r$ is the estimated speed in transient condition and ωr is the actual rotor speed, the position error can be derived from speed error as (12).

$$\theta_{error} = (\widehat{\omega} r - \omega r)t \tag{12}$$

Now,

$$i_{sd}^e = i^e{}_{sd} \sin\theta_{error} + i^e{}_{sq} \cos\theta_{error} \Rightarrow \Delta i_{sd}^e = \left(\frac{\partial i_{sd}^e}{\partial \theta_{error}}\right)\Delta\theta_{error} \tag{13}$$

at steady state, when $\theta_{error} = 0$ and $\widehat{\omega} r = \omega_r$, from (7) and (8).

$$\Delta i_{sd}^e = i_{sd0}^e \Delta\theta_{error} \tag{14}$$

Substituting (14) in (11),

$$\Delta\xi = \frac{3}{2} V_{pd0}^e i_{sd0}^e \Delta\theta_{error} \tag{15}$$

now, $\theta error = \int(\widehat{\omega} r - \omega r)dt$. Therefore,

$$\Delta\theta_{error}(s) = \frac{(\Delta\widehat{\omega}_r(s) - \Delta\omega_r(s))}{s} \tag{16}$$

Substituting from (12) in (10),

$$\Delta\xi = \frac{3}{2}\left[\frac{(\Delta\widehat{\omega}_r(s) - \Delta\omega_r(s))V_{pd0}^e i_{sd0}^e}{s}\right] \tag{17}$$

considering, Kp and Ki are the proportional and integral constants of PI- controller respectively. The open loop transfer function of the presented small signal model can be written as, $G(s)\,H(s) = \frac{3}{2}\frac{V_{pd0}^e i_{sd0}^e}{s}\left[K_p + K_i/s\right]$, and $G(s)\,H(s) = \frac{K_1}{s}\left[K_p + K_i/s\right]$. Where,

$$K_1 = \frac{3}{2} V_{pd0}^e i_{sd0}^e \tag{18}$$

using expression in (18), a root-locus has been drawn as shown in Figure 7. It can be observed that a double pole exists at origin and single zero exists at $-K_i/K_p$. Since the root-locus remains in left half of the S-plane, the proposed MRAS model is highly stable against any noise disturbances.

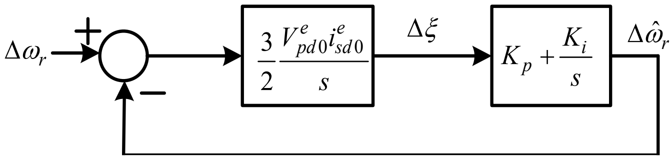

Figure 6. The small signal model of the proposed estimator with PI controller

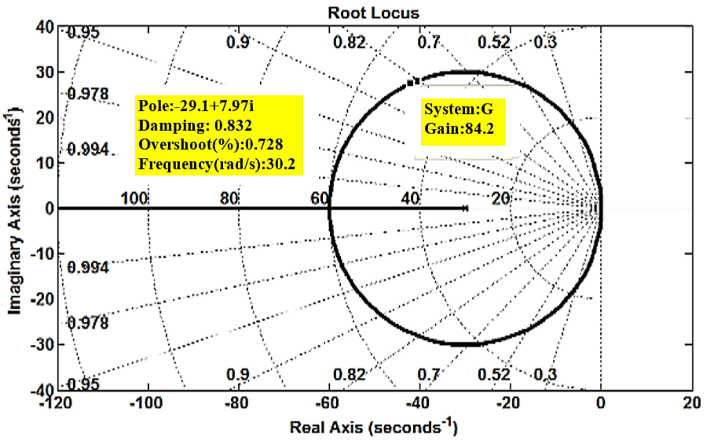

Figure 7. Root-locus of the small signal model

3. EXPERIMENT AND PERFORMANCE ANALYSIS

The proposed sensorless control scheme for the BDFRG has been initially designed using the MATLAB-Simulink platform to test the performance. The output has already been presented in the previous sections of this paper. To validate the MATLAB platform results and to test performance further, the proposed scheme has been implemented using hardware, as shown in Figure 8. For testing purposes, to create voltage flickers at PCC, both load and torque output of the wind turbine emulator have been quickly and systematically varied. The test results of the scaled prototype of the proposed scheme are shown in Figures 9(a)-9(h). The proposed sensorless control scheme is implemented using a PC-interfaced dSPACE CP1104 module and a 2.5 kW BDFRG. A two-channel DSO (100 kHz) has been used to capture the feasible significant test results. A 5 kW AC source has been used to represent the microgrids along with the necessary loading (R-L) arrangement. The effect of wind speed fluctuation has been emulated with the help of a prime mover (5 kW, torque-controlled, separately excited DC motor).

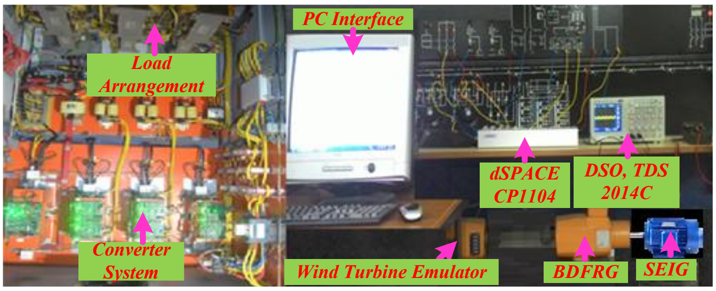

Figure 8. Outline of the experiment

As it has already been shown that the proposed sensorless control technique is stable against the noise disturbances, robust against machine parameter variations, and unbiased to voltage flickering at the PCC. The same can be observed from the test results shown in Figures 9(a) and 9(b). The voltage at the PCC has been varied by 50% for 1 ms through an overloading approach at the microgrids, and the recorded rotor position and the speed of the machine are presented in Figures 9(a) and 9(b), respectively. It can be observed that the proposed sensorless control scheme very accurately computes the BDFRG rotor position and the speed. As it has already been said, the accuracy of the active power generation is highly dependent on the accuracy of the controller. The active power generation from the BDFRG under voltage flickering at the PCC can be observed from Figure 9(c). It can be observed that the proposed sensorless controller provides robust performance under voltage flickering at the PCC. However, to test the DC-link performance, some more test results are presented here for the readers reference and understanding. To maintain 1 p.u. of active power at the primary winding terminals, the secondary winding active power fluctuates in synchronous with the wind turbine output power variations. Thus, the net active power exchange between the WECS and microgrids will vary according to the wind speed and, hence, the BDFRG rotor speed. The same can be observed in Figures 9(d) and 9(e).

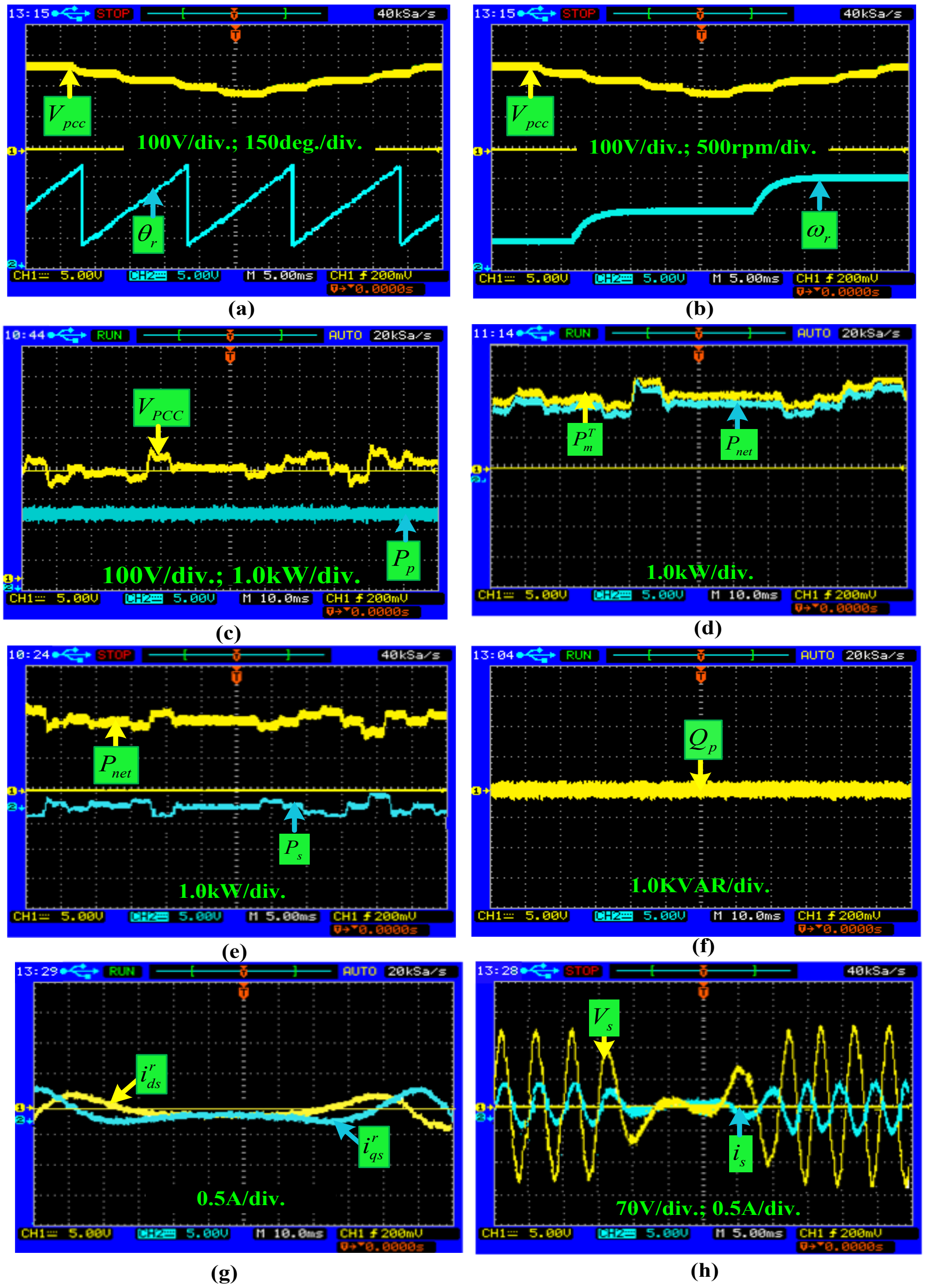

Figure 9. Performance of the planned MRAS embedded controller: (a) estimation of BDFRG rotor position, (b) estimation of BDFRG rotor speed, (c) accuracy of active power generation under voltage flickering at PCC, (d) control winding real power versus net active power generation, (e) DBDFRG rotor speed versus the primary winding active power, (f) reactive power loading, (g) dq control wing current, and (h) voltage and currents of control winding

Grid-side converter, as shown in Figure 1, plays a very important role in the above power exchange process. Though the controller part of the GSC is hidden in the literature, practically it has been implemented through two control loops, considering the DC-link voltage and the unit power factor $(Q_p = 0)$ as the reference variables. The mentioned control loop for the GSC helps to maintain a constant voltage at the DC-link and operate the WECS at the unit power factor, as observed in Figure 9(f).

During the BDFRG speed transition from subsynchronous to supersynchronous operation, the controller is required to perform effectively, particularly near synchronous speed. At this operating point, the slip becomes zero, resulting in an almost zero frequency of the control winding voltage and current. Consequently, the d–q axis currents of the control winding exhibit nearly DC behavior, as shown in Figure 9(g) indicates the effective performance of the controller during the speed transition.

In the subsynchronous operating region, the active power generation capability of the BDFRG is lower than the rated value. To maintain rated power generation at the primary winding terminals, the deficit power is injected through the control winding via the DC-link, leading to an almost zero phase angle between the control winding voltage and current. Conversely, in the supersynchronous operating region, both windings deliver power to the microgrids, resulting in $P_{net} > 1.0\ p.u.$ In this case, active power reversal occurs through the control winding, and the phase angle between the control winding voltage and current becomes approximately 180°, as illustrated in Figure 9(h).

A comparative analysis of the proposed sensorless scheme through test results as per IEEE Std 1453-2015 has been presented in Table 1. A standard voltage flickering at the PCC with $\frac{\Delta V}{V} \leq 0.5$ for 1 ms has been considered for testing purposes. It can be observed that the accuracy associated with the proposed sensorless scheme is comparatively high.

Table 1. BDFRG rotor position computation error against voltage flickering at PCC

$\frac{\Delta V}{V}$at PCC For 1ms	$\hat{\theta}_r$ error for proposed model (rad.)	% of P_p deviation for the proposed scheme	$\hat{\theta}_r$ error for primary winding flux based MRAS (rad.) [25]	% of P_p deviation for the scheme in [25]	$\hat{\theta}_r$ error for active power based MRAS (rad.) [26]	% of P_p deviation for the scheme in [26]
-50%	-0.008	-0.016	0.109	-1.500	0.160	-1.600
-40%	-0.007	-0.015	0.088	-1.300	0.150	-1.500
-30%	-0.005	-0.013	0.070	-1.200	0.120	-1.400
-20%	-0.003	-0.012	0.054	-1.000	0.094	-1.300
-10%	-0.001	-0.010	0.032	-0.900	0.049	-1.200
0%	0.000	0.000	0.000	0.000	0.000	0.000
+10%	0.001	0.010	-0.034	0.900	-0.064	1.200
+20%	0.002	0.012	-0.054	1.000	-0.089	1.300
+30%	0.002	0.013	-0.076	1.200	-0.138	1.400
+40%	0.003	0.015	-0.094	1.300	-0.138	1.500
+50%	0.004	0.016	-0.117	1.500	-0.168	1.600

4. CONCLUSION

The proposed sensorless control mechanism for the brushless doubly fed reluctance generator, sustainable to the voltage flickers at the PCC, has been successfully implemented, and feasible test results have been presented in this paper. It has been observed that the proposed sensorless control scheme is not sensitive to the machine parameter variations. The performance of the model has been tested for a 50% variation in magnetizing inductance of the brushless doubly-fed reluctance generator (BDFRG) and found that the proposed MRAS model computes rotor position and rotor speed with insignificant errors. The test result reveals that the MRAS model is sustainable to the voltage flickers $\frac{\Delta V}{V} \leq 0.5$ for 1 ms at PCC. The active power variation due to the error associated with the proposed BDFRG rotor position computation is found to be 0.016%, which is negligible in comparison to the 1.6% for the other similar schemes. The stability of the model against noise disturbance has been analyzed, and found that the model exhibits robust performance against the noise disturbances. The performance of the proposed controller for SSG has been recorded and successfully presented in this paper.

FUNDING INFORMATION

Authors state no funding involved.

AUTHOR CONTRIBUTIONS STATEMENT

This journal uses the Contributor Roles Taxonomy (CRediT) to recognize individual author contributions, reduce authorship disputes, and facilitate collaboration.

Name of Author	C	M	So	Va	Fo	I	R	D	O	E	Vi	Su	P	Fu
Manish Paul		✓	✓	✓	✓	✓		✓	✓	✓	✓		✓	
Adikanda Parida	✓			✓	✓	✓		✓	✓	✓		✓		✓
Anu Kumar Das	✓	✓	✓				✓	✓	✓	✓	✓		✓	

C : **C**onceptualization
M : **M**ethodology
So : **So**ftware
Va : **Va**lidation
Fo : **Fo**rmal analysis
I : **I**nvestigation
R : **R**esources
D : **D**ata Curation
O : Writing - **O**riginal Draft
E : Writing - Review & **E**diting
Vi : **Vi**sualization
Su : **Su**pervision
P : **P**roject administration
Fu : **Fu**nding acquisition

CONFLICT OF INTEREST STATEMENT

Authors state no conflict of interest.

DATA AVAILABILITY

Data availability is not applicable to this paper as no new data were created or analyzed in this study.

REFERENCES

[1] M. G. Jovanovic, "Theoretical analysis of control properties for the brushless doubly fed reluctance machine," *IEEE Power Engineering Review*, vol. 22, no. 7, p. 49, 2002, doi: 10.1109/MPER.2002.4312352.

[2] S. Khaliq, M. Modarres, T. A. Lipo, and B. Il Kwon, "Design of novel axial-flux dual stator doubly fed reluctance machine," *IEEE Transactions on Magnetics*, vol. 51, no. 11, 2015, doi: 10.1109/TMAG.2015.2444382.

[3] F. Wang, F. Zhang, and L. Xu, "Parameter and performance comparison of doubly-fed brushless machine with cage and reluctance rotors," in *Conference Record of the 2000 IEEE Industry Applications Conference. Thirty-Fifth IAS Annual Meeting and World Conference on Industrial Applications of Electrical Energy (Cat. No.00CH37129)*, IEEE, 2002, pp. 539–544, doi: 10.1109/IAS.2000.881162.

[4] L. Xu, L. Zhen, and E. H. Kim, "Field-orientation control of a doubly excited brushless reluctance machine," *IEEE Transactions on Industry Applications*, vol. 34, no. 1, pp. 148–155, 1998, doi: 10.1109/28.658739.

[5] A. M. Knight, R. E. Betz, and D. G. Dorrell, "Design and analysis of brushless doubly fed reluctance machines," *IEEE Transactions on Industry Applications*, vol. 49, no. 1, pp. 50–58, 2013, doi: 10.1109/TIA.2012.2229451.

[6] S. Ademi and M. Jovanovic, "Control of doubly-fed reluctance generators for wind power applications," *Renewable Energy*, vol. 85, pp. 171–180, 2016, doi: 10.1016/j.renene.2015.06.040.

[7] M. R. A. Kashkooli and M. G. Jovanović, "Sensorless adaptive control of brushless doubly-fed reluctance generators for wind power applications," *Renewable Energy*, vol. 177, pp. 932–941, 2021, doi: 10.1016/j.renene.2021.05.154.

[8] M. Jovanovic, "Sensored and sensorless speed control methods for brushless doubly fed reluctance motors," *IET Electric Power Applications*, vol. 3, no. 6, pp. 503–513, 2009, doi: 10.1049/iet-epa.2008.0227.

[9] M. G. Jovanovic, R. E. Betz, and J. Yu, "The use of doubly fed reluctance machines for large pumps and wind turbines," in *Conference Record - IAS Annual Meeting (IEEE Industry Applications Society)*, 2001, pp. 2318–2325, doi: 10.1109/ias.2001.955947.

[10] M. Jovanovic, "Sensored and sensorless speed control methods for brushless doubly fed reluctance motors," *IET Electric Power Applications*, vol. 3, no. 6, pp. 503–513, 2009, doi: 10.1049/iet-epa.2008.0227.

[11] M. G. Jovanović, J. Yu, and E. Levi, "Encoderless direct torque controller for limited speed range applications of brushless doubly fed reluctance motors," *IEEE Transactions on Industry Applications*, vol. 42, no. 3, pp. 712–722, 2006, doi: 10.1109/TIA.2006.872955.

[12] S. Liang, S. Jin, and L. Shi, "Research on control strategy of grid-connected brushless doubly-fed wind power system based on virtual synchronous generator control," *CES Transactions on Electrical Machines and Systems*, vol. 6, no. 4, pp. 404–412, 2022, doi: 10.30941/CESTEMS.2022.00052.

[13] M. Kumar, S. Das, and K. Kiran, "Sensorless speed estimation of brushless doubly-fed reluctance generator using active power based MRAS," *IEEE Transactions on Power Electronics*, vol. 34, no. 8, pp. 7878–7886, 2019, doi: 10.1109/TPEL.2018.2882473.

[14] M. Paul and A. Parida, "Maximization of active power delivery in WECS using BDFRG," *Springer Proceedings in Mathematics and Statistics*, vol. 417, pp. 259–265, 2023, doi: 10.1007/978-3-031-25194-8_21.

[15] M. R. A. Kashkooli and M. G. Jovanovic, "A MRAS observer based sensorless control of doubly-fed reluctance wind turbine generators," in *IECON 2020 The 46th Annual Conference of the IEEE Industrial Electronics Society*, IEEE, Oct. 2020, pp. 1734–1739, doi: 10.1109/IECON43393.2020.9255202.

[16] A. Parida, S. Choudhury, and D. Chatterjee, "Microgrid based hybrid energy co-operative for grid-isolated remote rural village power supply for east coast zone of India," *IEEE Transactions on Sustainable Energy*, vol. 9, no. 3, pp. 1375–1383, 2018, doi: 10.1109/TSTE.2017.2782007.

[17] A. Parida and D. Chatterjee, "Cogeneration topology for wind energy conversion system using doubly-fed induction generator," *IET Power Electronics*, vol. 9, no. 7, pp. 1406–1415, 2016, doi: 10.1049/iet-pel.2015.0581.

[18] A. Parida and D. Chatterjee, "Stand-alone AC-DC microgrid-based wind-solar hybrid generation scheme with autonomous energy exchange topologies suitable for remote rural area power supply," *International Transactions on Electrical Energy Systems*, vol. 28, no. 4, 2018, doi: 10.1002/etep.2520.

[19] A. Parida and D. Chatterjee, "Integrated DFIG–SCIG-based wind energy conversion system equipped with improved power generation capability," *IET Generation, Transmission & Distribution*, vol. 11, no. 15, pp. 3791–3800, Oct. 2017, doi: 10.1049/iet-gtd.2016.1246.

[20] S. J. Rind, Y. Ren, K. Shi, L. Jiang, and M. Tufail, "Rotor flux-MRAS based speed sensorless non-linear adaptive control of induction motor drive for electric vehicles," in *2015 50th International Universities Power Engineering Conference (UPEC)*, IEEE, Sep. 2015, pp. 1–6, doi: 10.1109/UPEC.2015.7339869.

[21] M. Rashed and A. F. Stronach, "A stable back-EMF MRAS-based sensorless low-speed induction motor drive insensitive to stator resistance variation," *IEE Proceedings: Electric Power Applications*, vol. 151, no. 6, pp. 685–693, 2004, doi: 10.1049/ip-epa:20040609.

[22] A. V. R. Teja, V. Verma, and C. Chakraborty, "A new formulation of reactive-power-based model reference adaptive system for sensorless induction motor drive," *IEEE Transactions on Industrial Electronics*, vol. 62, no. 11, pp. 6797–6808, 2015, doi: 10.1109/TIE.2015.2432105.

[23] A. V. R. Teja, C. Chakraborty, S. Maiti, and Y. Hori, "A new model reference adaptive controller for four-quadrant vector-controlled induction motor drives," *IEEE Transactions on Industrial Electronics*, vol. 59, no. 10, pp. 3757–3767, 2012, doi: 10.1109/TIE.2011.2164769.

[24] K. Kiran, S. Das, M. Kumar, and A. Sahu, "Sensorless speed control of brushless doubly-fed reluctance motor drive using secondary flux based MRAS," *Electric Power Components and Systems*, vol. 46, no. 6, pp. 701–715, 2018, doi: 10.1080/15325008.2018.1466006.

[25] M. Kumar, S. Das, and K. Kiran, "Sensorless speed estimation of brushless doubly-fed reluctance generator using active power based MRAS," *IEEE Transactions on Power Electronics*, vol. 34, no. 8, pp. 7878–7886, 2019, doi: 10.1109/TPEL.2018.2882473.

[26] J. F. Silva and S. F. Pinto, *Power Electronics Handbook: Circuits, Devices, and Applications*. 3rd ed. Elsevier, 2011.

[27] R. Krishnan, *Electric Motor Drives: Modeling, Analysis and Control*, 1st ed. Pearson Education, 2003.

BIOGRAPHIES OF AUTHORS

Manish Paul received the Ph.D. in electrical engineering from NERIST, Arunachal Pradesh, in 2024. He is currently working as an assistant professor in the Department of Electrical Engineering, ICFAI University, Tripura, India. His research interests include electric motor drives, wind energy conversion, control of doubly fed machines for variable speed applications, and reluctance machines. He can be contacted at email: manishpaul1988@gmail.com.

Adikanda Parida received the Ph.D. degree in Electrical Engineering Department from Jadavpur University, Kolkata, India. His research interests include hybrid renewable power generation, rural electrification, energy conservation, and management. He is a member of IEEE. He can be contacted at email: adikanda_2003@yahoo.co.in.

Anu Kumar Das received the Ph.D. degree from North Eastern Regional Institute of Science and Technology, Nirjuli, India. His research interests include power systems and high voltage. He can be contacted at email: akdnerist@gmail.com.